

Design and characterization of a scaled-up ultrasonic flow reactor

Claire Delacour¹, Dwayne S. Stephens², Cecile Lutz³, Robert Mettin², Simon Kuhn^{1}*

¹KU Leuven, Department of Chemical Engineering, Celestijnenlaan 200F, 3001 Leuven,
Belgium

²Drittes Physikalisches Institut, Georg-August-Universität Göttingen, Friedrich-Hund-Platz 1,
37077 Göttingen, Germany

³Service Adsorption, ARKEMA, Groupement de Recherche de Lacq, 64170 Lacq, France

Abstract: Ultrasonic microreactors are increasingly applied to particle synthesis, crystallization processes, or organic synthesis involving solids due to the clogging prevention offered by ultrasound irradiation. However, the further application of this technology is limited by the scalability of ultrasonic flow reactors. In this work, we combined experiments and numerical simulations for the design of a scaled-up flow reactor. The reactor consists of a perfluoroalkoxy alkane (PFA) tubing immersed in a box to transmit the ultrasound and provide temperature control, to which six Langevin multifrequency transducers are attached. The acoustic pressure distribution was investigated to characterize the effect of ultrasound frequency and the transducer configurations on particle size distribution for the model reaction of barium sulfate synthesis. Operating the scaled-up reactor with six transducers at a frequency of 40 kHz resulted in an acoustic wave distribution with maximum acoustic pressures in the vicinity of the tubular reactor, thus leading to a small particle size distribution and consequently clogging prevention. The productivity of the scaled-up reactor was 14g/h barium sulfate at a remarkably low applied ultrasound power of 0.48W/mL, highlighting the efficient design and the further scale-up potential.

Keywords: Ultrasound, flow reactor, scale-up, clogging prevention

1. Introduction

The synergistic effect of combining ultrasound with micro- and milli-fluidic devices allows to expand their application range for continuous manufacturing. Ultrasonic microreactors have already shown some interesting results for the synthesis of particles¹⁻⁷, crystallization processes⁸ or for organic synthesis applications⁹⁻¹⁴. Depending on the applied frequency, different phenomena resulting in clogging prevention are occurring. From 20 to 100kHz, low frequency ultrasound

effects are driven by a high cavitation activity, and shear forces induced by the collapse of the cavitation bubbles results in agglomerate break-up. High frequency ultrasound effects (above 1MHz) are driven by acoustic streaming, and clogging is prevented by centering particles in the flow channel^{2,7,15}.

However, the applicability of the combination of ultrasound with micro- and milli-fluidic devices is still limited to academic research¹⁵. To make this combination viable for industry, it needs to provide (1) a high production rate and (2) to keep the same product quality during the process. Thus, methods to scale-up such reactors need to be developed, where the aim is to retain the advantages of micro- and milli-reactors and to control the acoustic pressure field distribution across scales. The fluidic part of an ultrasonic reactor can be scaled via two approaches, *i.e.* scaling out and numbering up. Scaling out is based on increasing the characteristic dimensions of the reactor. This approach has been used by John *et al.*¹⁶ for the design of an interval contact reactor for liquid-liquid separation. The reactor consists in an ultrasonic bath, with interval metal plates inserted. Those plates are in direct contact with the reactor tubing. John *et al.* compared the obtained mass transfer coefficients for a liquid-liquid extraction with a 0.8mm and a 2mm inner diameter tubing. Results showed that increasing the inner diameter to 2mm allowed to increase the mass transfer by 14-20%. Numbering up on the other hand is based on operating several identical units in parallel or in series^{17,18}. This approach has been used by Verhaagen *et al.*¹⁹⁻²¹ for the design of a cavitation intensification bag for emulsification applications. The reactor system consists of plastic bags immersed in an ultrasonic bath in parallel. The volume of each plastic bag was between 11mL and 15mL. In contrast, Ezeanovi *et al.*^{22,23} developed a process for the continuous sonocrystallization of phtalic acid in three jacketed reactor units in series. Each unit is composed of a tubing of 8mm inner diameter and 16m length coiled around a 25kHz sonotrode. Scale-up is

also achieved by combining the scaling out and numbering up approach. Karvonen *et al.* patented a sonocrystallization process reactor²⁴ composed of different crystallization units. Those units are composed of a tubing coiled in a circulating bath for temperature control. Transducers are connected at the bottom of each bath ensuring an indirect coupling between the ultrasonic source and the reactor tubing. The process was designed with modifiable parameters such as length, diameter of the tubing or number of reactor units, and can be applied to cooling crystallization or anti-solvent crystallization.

In addition to the scale-up of the fluidic part of an ultrasonic reactor, it is also required to characterize the primary and secondary effects of low frequency ultrasound across scales^{15,25–28}. To date, there are few studies that have investigated characterization methods of ultrasonic effects in micro and milli-fluidic devices^{15,20,29–32}. The main investigated parameter is the acoustic pressure field distribution^{20,28,29,31–33}. This parameter can be characterized by using both experiments and numerical simulation. Hydrophone measurements of the acoustic pressure^{20,32} and sonochemiluminescence observations, based on the reaction between luminol and hydroxyl radicals formed by ultrasonic cavitation^{15,31,32}, were carried out by Verhaagen *et al.*²⁰ for the design and characterization of their cavitation intensification bag setup, which enabled to place the cavitation bag at the most active site in the ultrasonic bath. In contrast, Jamshidi *et al.*³⁰ designed an ultrasonic flow reactor for crystallization of adipic acid with the help of numerical simulations³⁰, where the cavitation probability in the reactor was determined by solving the wave propagation equation. The scaled-out reactor consists of a glass chip with an etched channel ($W \times L \times H = 2\text{mm} \times 76\text{mm} \times 5\text{mm}$) directly attached to a piezoelectric plate. These examples highlight the importance of including ultrasound characterization to design efficient reactors.

In this work, we develop a scaled-up ultrasonic reactor to prevent clogging in particle forming reactions. The developed reactor was designed with flexibility in the applied frequency and configuration of the transducers relative to the reactor. These different parameters were characterized with the use of experiments and numerical simulations to identify the optimum configuration for particle synthesis under flow conditions. Finally, the achieved increase in productivity of the best configuration is assessed by comparison with an ultrasonic micro-reactor.

2. Materials and methods

2.1. Experimental set-up

The reactor assembly is shown in Figure 1, and it consists of a box (cavity dimensions: 150x40x40mm³) connected to ultrasound transducers which circulates a heat and sound transfer fluid and in which a tubular reactor is embedded. This box is either made out of polycarbonate to allow optical access for the characterization of the acoustic field distribution or aluminum for chemical synthesis (barium sulfate precipitation reaction). Up to six Langevin's type transducers (Steminc SMLTF4080W50) operated at either 40 kHz or 80 kHz can be attached to the box. Silicon oil is circulated using a heat transfer bath (Julabo HC) through the box to control the temperature of the tubular reactor. The tubular reactor made of PFA with an inner diameter of 2mm, outer diameter of 3mm and a length of 3.81 m (internal volume 12mL), is wrapped as a helix and inserted in the box (see Figure 1b). The thickness of the box where the transducers are connected corresponds to an eighth wavelength or a sixteenth wavelength of the applied frequency in polycarbonate or aluminum. The six transducers are placed as such: two transducers per side on two opposite faces and 1 transducer per side on the other two faces of the box (see Figure 1a). To

control and provide ultrasound to the system, transducers are connected in parallel to a waveform generator (Rigol DG1032, 30MHz, 200MSa/s) and a power amplifier (E&I 1040L).

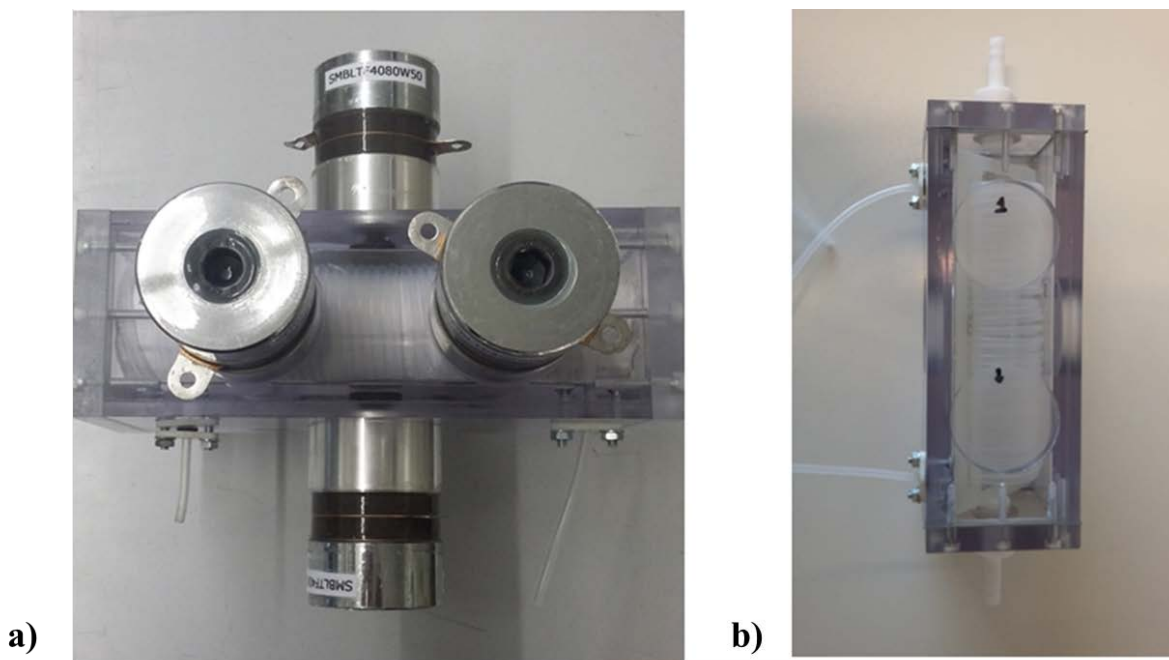


Figure 1. Picture of the scaled-up ultrasound reactor using the polycarbonate box. a) Top view of the reactor with the transducers attached to it. b) Top view of the reactor without transducers, showing the coiled reactor tubing inside the box.

2.2. Characterization of the reactor

2.2.1. Impedance analysis

An impedance analysis was carried out to determine the resonance mode of the reactor using a Sinephase 16777k impedance analyzer. Two main frequencies were observed, the first one is around 40kHz and the second one is around 80kHz. These frequencies are found for both the polycarbonate and the aluminum reactor, and when measuring individual transducers and the transducer assembly.

2.2.2. Sonochemiluminescence observation

The distribution of the pressure field was observed by the sonochemiluminescence of luminol. This method is based on the reaction between 3-aminophthalhydrazide, also called luminol, and hydroxyl radicals formed by cavitation bubbles in sonicated water. The luminol solution is prepared by dissolving 0.84g of sodium hydroxide (Acros Organics, pellets), with 0.35g of luminol (TCI chemicals, 98%) in 200mL milli-Q water. The result of this reaction is the emission of blue light, and the observation of the spatial distribution of the light intensity allows the characterization of pressure nodes and antinodes. Pictures were taken through one of the surfaces of the box where only a single transducer is attached, with a trigger time of 30s using a Nikon Camera D810. The ISO norm, to control the light sensitivity of the camera sensor, was adjusted depending on the operating conditions.

2.2.3. Hydrophone measurements

Hydrophone measurements were made to further characterize the acoustic pressure distribution inside the polycarbonate reactor. As the top of the polycarbonate reactor could be removed, 2D maps of the acoustic pressure could be obtained, and two different hydrophones were used to map the pressure when the reactor was filled with water. The first hydrophone (Onda HNR-0500, USA further referred to as MHz hydrophone) was calibrated for the range of 0.25 to 10 MHz and connected to a digital oscilloscope (Tektronix DPO 4104, USA). Due to its small diameter (~2mm) it has a high spatial resolution and was therefore used to make 2D profiles of the acoustic pressure distribution. Since the actuation frequency was well below the MHz range this hydrophone cannot determine the absolute pressure. Hence, to quantify the pressure magnitude, a second hydrophone (further referred to as kHz hydrophone) was used (Brüel & Kjaer 8103, Denmark). This hydrophone is calibrated between 0.1 to 180 kHz and was connected to a digital oscilloscope

(Keysight DS0X1102A, Digital Storage Oscilloscope, 70MHz - 2GSa/s). The pressure measurements were recorded in the center of the reactor where the maximum pressure was observed. It should be noted that measurements made with the MHz hydrophone were made at a very low input power $\sim 1\text{W}$ so that cavitation would not interfere with the measurement and also to avoid damaging the sensitive tip.

2.2.4. COMSOL simulation

The numerical model uses a nonlinear Helmholtz equation as described by Louisnard^{34,35} that accounts for thermal and viscous losses due to cavitation. Cavitating bubbles are homogeneously distributed in regions where pressure exceeds the Blake threshold. The void fraction is taken as $\beta = 4 \cdot 10^{-7}$ for 40kHz and $\beta = 4 \cdot 10^{-6}$ for 80kHz. The bubble rest radius was set to $R_0 = 3\mu\text{m}$ for both frequencies. These void fractions were chosen to match the experimentally measured pressure at the center of the reactor. Those particular values are chosen because in a linear case ($\beta = 0$) the simulated pressure is unrealistically high and does not correlate with pressure measurements³¹. The 3D acoustic field is calculated for the liquid as well as for the solid walls of the reactor using the pressure acoustics module in COMSOL (Comsol AB, Stockholm). The solid walls are effectively treated as a dense fluid. In reality, however, acoustic waves travel through solids in the form of elastic body waves (P-waves and S-waves). This more complex acoustic-structure interaction is omitted because the results between simulation and experiments are in close agreement despite this simplified wall treatment. Sound-soft boundary conditions are applied on all external surfaces. A pressure condition $P = \sqrt{\frac{2\rho_B c_B P_{diss}}{A_{trans}}}$ ^{29,36,37} is applied on the transducer-wall interface with ρ_B and c_B being the density and speed of sound in the solid reactor material. P_{diss} is the power delivered to each transducer and A_{trans} is the irradiating surface of each

transducer. Sound-soft boundary conditions are applied to all remaining free surfaces. Table 1 summarizes the different materials properties used in the COMSOL simulations.

Table 1. Properties of materials and liquids used in the COMSOL simulations

Parameter	Value	Unit
Polycarbonate		
Density	1220	kg/m ³
Speed of sound	2700	m/s
Aluminum		
Density	2700	kg/m ³
Speed of sound	6320	m/s
Silicone oil		
Surface tension	0.02	N/m
Vapour pressure	666.67	Pa
Dynamic viscosity	0.097	Pa.s
Speed of sound	1350	m/s
Density	967	kg/m ³
Water		
Surface tension	0.0725	N/m
Vapour pressure	2330	Pa
Dynamic viscosity	0.001	Pa.s
Speed of sound	1500	m/s
Density	1000	kg/m ³

2.2.5. Barium sulfate precipitation

The barium sulfate precipitation was chosen as a model reaction. Barium sulfate particles are formed by mixing aqueous solutions of barium chloride ($\text{BaCl}_2 \cdot 2\text{H}_2\text{O}$, Flasher Chemical, Laboratory reagent grade, 0.5M) and sodium sulfate (Na_2SO_4 , Merck, 99% purity, 0.5M). HPLC pumps (LD class, Instrument selections) were used to deliver the reactants, for this study, the flow rate of each reactant was fixed at 1mL/min. Before and after each experiment, the reactor is washed with a saturated solution of sodium carbonate (Na_2CO_3 , Acros Organics, 99.5% purity) and then with acetic acid (ChemLab, 99-100% purity). The reactor is carefully rinsed to remove any traces of acid. To study the impact of ultrasonic parameters on barium sulfate particles, samples are collected at the outlet of the reactor for two purposes: (1) yield measurements and (2) particle size distribution. For yield measurement, samples are collected for 30s each 6min. This period between two measurements was chosen to correspond to a through flow of one reactor volume. Measurements showed that steady state is reached after 3 reactor volumes. The obtained yield after 3 reactor volumes are then averaged. This yield measurement also allows to determine the stability of the process. In contrast, for samples for particle size distribution analysis, only few droplets are collected. Those droplets are then added to the 7mL cell of the Mastersizer (Malvern hydro SV) for analysis. Two ways to represent particle size distribution are shown in this paper. The first one represents the Gauss volume distribution in particle sizes while the second one gathers the characteristic sizes $D_v(10)$, $D_v(50)$ and $D_v(90)$ corresponding to 10, 50 and 90% of particles being below this certain size, respectively. On this second representation, the span of the distribution is also calculated as the difference between $D_v(90)$ and $D_v(10)$. This value is named as $D_v(90-10)$. Figure 2 depicts the experimental setup used in this work.

The effect of different ultrasonic parameters (applied frequency, transducer configuration) on the particle size distribution and reaction yield were investigated and compared to results obtained without applying ultrasound, called silent conditions. Figure 3 shows the studied ultrasonic frequency configurations and Figure 4 depicts the studied transducer configurations at a fixed frequency of 40kHz.



Figure 2. Photograph of the experimental setup. The polycarbonate reactor is connected to a heat transfer bath circulating silicon oil, HPLC pumps are used to deliver the reactants and a temperature sensor is connected to the reactor outlet. An air fan is used to cool the transducer temperature.

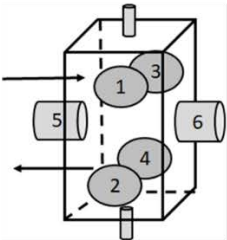
Configuration	6tr-40	6tr-80	6tr-40/80
	1. 40kHz	1. 80kHz	1. 40kHz
	2. 40kHz	2. 80kHz	2. 80kHz
	3. 40kHz	3. 80kHz	3. 80kHz
	4. 40kHz	4. 80kHz	4. 40kHz
	5. 40kHz	5. 80kHz	5. 40kHz
	6. 40kHz	6. 80kHz	6. 80kHz

Figure 3. Studied frequency configurations: in case A all 6 transducers are operating at 40kHz, in case B all 6 transducers are operating at 80kHz, in case C, 3 transducers are operating at 40kHz and the other 3 at 80kHz: opposing transducers have different frequencies.

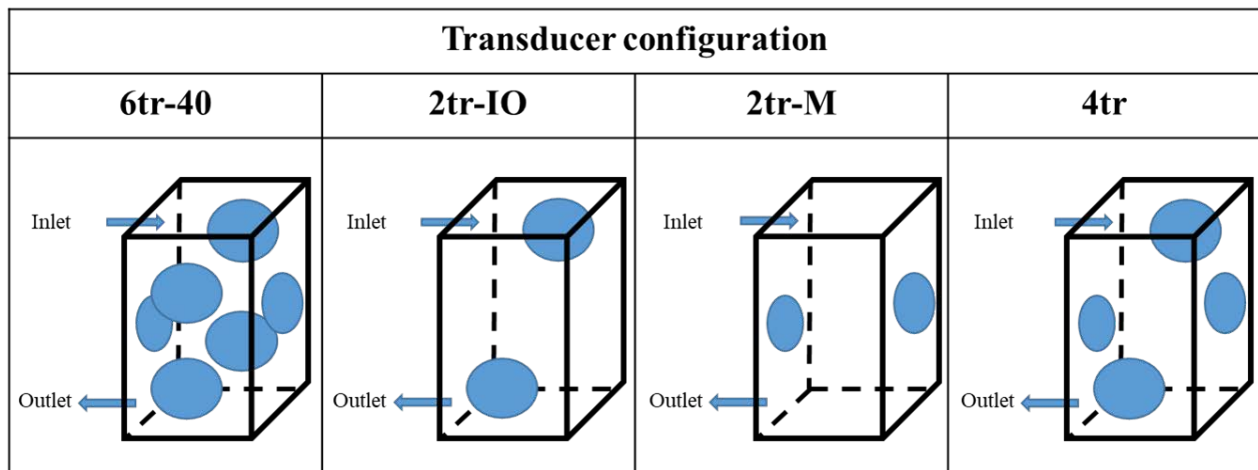


Figure 4. Studied transducer configurations: a) 6tr-40 corresponds to the case where all 6 transducers are used; b) 2tr-IO corresponds to the case where only 2 transducers are used, one close to the inlet and the second close to the outlet; c) 2tr-M corresponds to the case where only two transducers are used in the middle of the reactor; d) 4tr corresponds to the case where two transducers are used in the middle of the reactor and two are used at the inlet and outlet of the tubing.

3. Results and discussions

3.1. Characterization of the reactor

The scaled-up reactor design was characterized using experimental and numerical methods. The aim was to use the mathematical model of the reactor to understand the effects of ultrasonic parameters on the barium sulfate synthesis. Figure 5 depicts the pressure amplitude at the center of the polycarbonate reactor filled with water for 37kHz, 40kHz and 41kHz with a total power ranging between 30W to 120W (5W to 20W delivered to each transducer). This frequency range corresponds to the range provided by the transducer supplier. The pressure varies between 2–2.4bar in the power range 60W to 100W, with the value slightly dropping as the power approaches 120W. This attenuation of sound energy is possibly due to the acoustic shielding caused by the formation of larger bubble clouds³⁸ in front of the transducers or near the hydrophone tip as the acoustic intensity is increased.

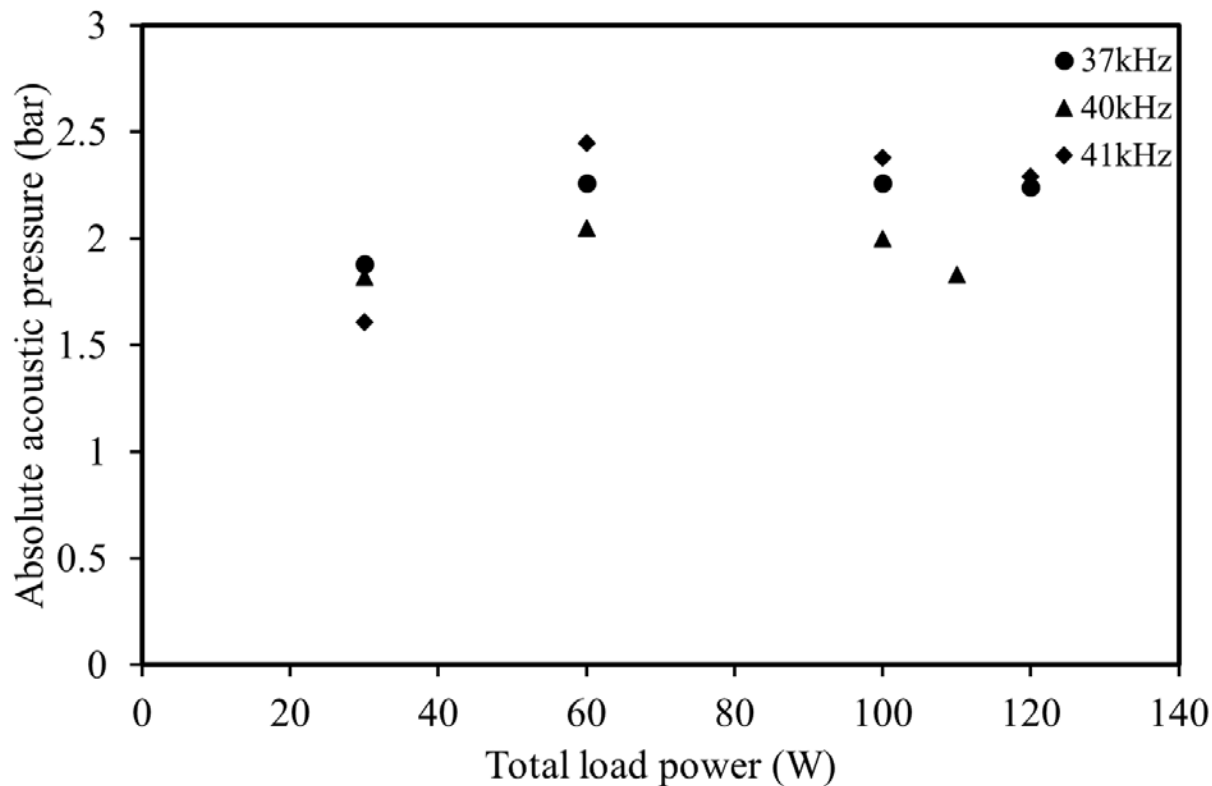


Figure 5. Absolute acoustic pressure at the center of the polycarbonate reactor filled with water for different applied ultrasound frequencies and load powers.

Figure 6 depicts the acoustic pressure mapping obtained experimentally by sonochemiluminescence, hydrophone measurements and COMSOL simulations in the polycarbonate reactor at a frequency of 40kHz.

As the hydrophone measurements were made with the top of the box open this was also taken into account in the simulation. Using the magnitude of acoustic pressure measured with the kHz hydrophone at the center at 120W, the 2D pressure distribution, measured with the MHz hydrophone, is linearly scaled such that the pressure in the center is 2bar. Comparing the hydrophone measurements with the simulation a good agreement in the spatial distribution and

maximum pressure is observed. This is also confirmed by the sonochemiluminescence observations. The three characterization methods allowed to observe the nodes and antinodes in the reactor, which are observed close to the box wall and in the center (see Figure 6f).

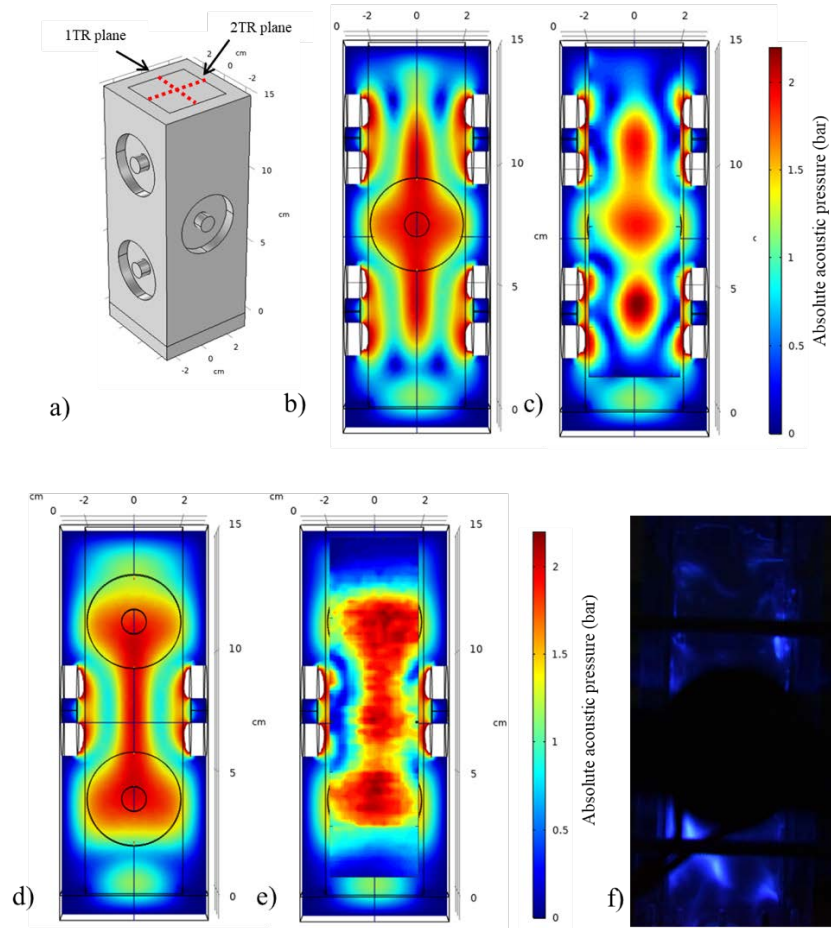


Figure 6. Characterization results for the 6tr-40 configuration. In the simulation, pressures above 2.4bar occur near the transducers and are omitted (colored white) and the same color bar is used. (a) Geometry of the polycarbonate reactor with an open top and the two planes of measurements. (b) 2TR plane of the simulated absolute acoustic pressure field with $\beta = 4 \cdot 10^{-7}$ and bubble rest radius $R_0 = 3\mu\text{m}$ irradiated at 120W (20W per transducer). (c) Overlay of the measured absolute acoustic pressure field at 120W on top of the simulated absolute acoustic pressure field. (d) 1TR plane of the simulated absolute acoustic pressure field irradiated at 120W (20W on each transducer) (e) Overlay of the measured absolute acoustic pressure field on top of the simulated field (f) 2TR plane sonochemiluminescence observation, obtained with the six transducers attached to the reactor at a load power of 213W.

3.2. Effect of the frequency configuration on the barium sulfate precipitation reaction

To investigate the effect of the frequency configuration on the acoustic pressure field distribution and on the barium sulfate precipitation reaction, experiments were conducted at 20W load power per transducer in the aluminum reactor and for the 6tr-40, 6tr-80 and 6tr-40/80 configuration (see Figure 3).

Figure 7 depicts the acoustic pressure distribution based on COMSOL simulations in the three frequency configurations. The pattern of nodes and antinodes is clearly visible for the single frequency cases, i.e. 6tr-40 (Figure 7a) and 6tr-80 (Figure 7b). As expected, more nodes and antinodes are observed when the frequency is increased from 40 to 80kHz. The simulations indicate larger acoustic pressures for the 6tr-80 case compared to the 6tr-40 case. This may be due to the assumption that bubbles with $R_0 = 3\mu m$ are seeded in both cases, whereas smaller cavitating bubbles are observed at higher frequencies. Louisnard^{34,35} shows higher viscous dissipation for a smaller cavitating bubble ($R_0 = 3\mu m$) as compared to a larger one ($R_0 = 8\mu m$). However, the node and antinode distribution is not clear in the 6tr-40/80 case (see Figure 7c), as transducers operating at different frequencies are facing each other, leading to interference of the acoustic waves. It is worth noting that large pressure values (<2bar) are obtained for all three configurations near the box surface where the tubing is located, ensuring a good coupling of ultrasound with the reaction mixture (see Figure 8).

a) 6tr-40**b) 6tr-80****c) 6tr-40/80**

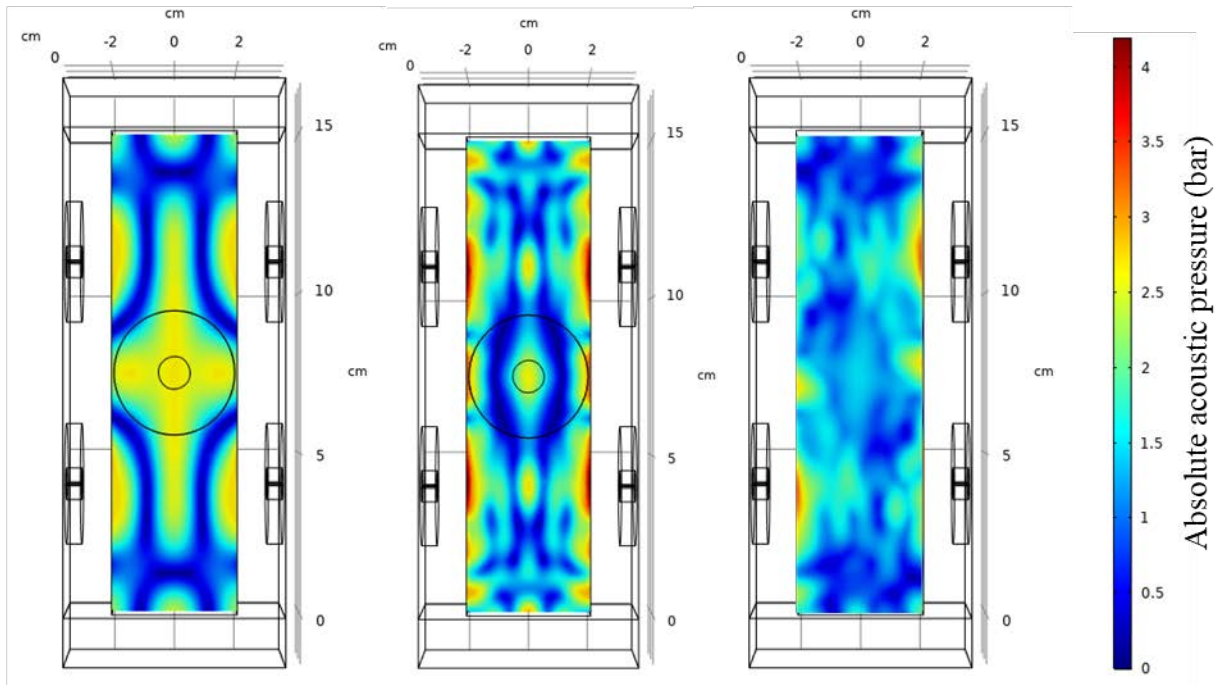


Figure 7. Contours of the absolute acoustic pressure field based on COMSOL simulations for a total power of 120W (20W per transducer) (a) 6tr-40 obtained with a void fraction of $\beta = 4 \cdot 10^{-7}$ (b) 6tr-80 obtained with a void fraction of $\beta = 4 \cdot 10^{-6}$ (c) 6tr-40/80 obtained with a void fraction of $\beta = 4 \cdot 10^{-7}$ for 40kHz and $\beta = 4 \cdot 10^{-6}$ for 80kHz.

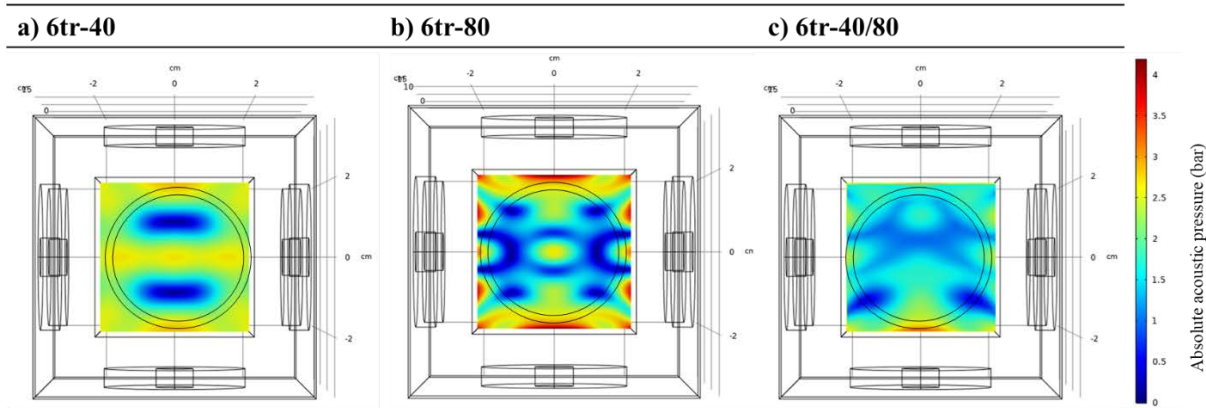
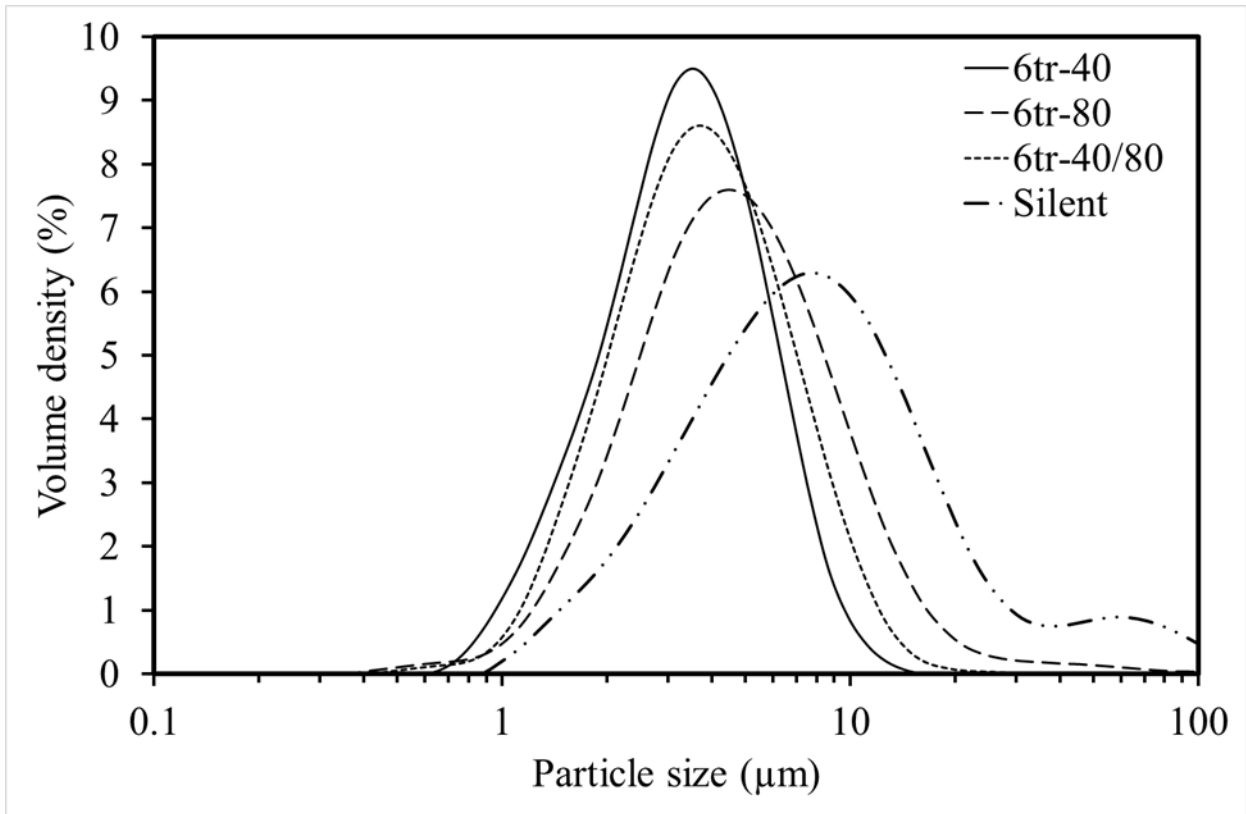


Figure 8. Contours of the absolute acoustic pressure field based on COMSOL simulations for a total power of 120W (20W per transducer) view from the top of the middle section of the reactor, tubing is represented with two circles (a) 6tr-40 (b) 6tr-80 (c) 6tr-40/80. (a) 6tr-40 obtained with a void fraction of $\beta = 4 \cdot 10^{-7}$ (b) 6tr-80 obtained with a void fraction of $\beta = 4 \cdot 10^{-6}$ (c) 6tr-40/80 obtained with a void fraction of $\beta = 4 \cdot 10^{-7}$ for 40kHz and $\beta = 4 \cdot 10^{-6}$ for 80kHz.

The experimentally obtained particle size distributions for the three frequency configurations, and as reference the silent condition, are shown in Figure 9. Upon sonication, the mean particle size and the span of the particle size distributions are reduced compared to the silent condition. This size reduction is caused by the breakup of particle agglomerates due to the collapse of cavitation bubbles^{1,6,9,39}. However, differences in the particle size distributions within the three studied frequency configurations are observed. The widest sizes distribution and largest mean size is obtained for the 6tr-80 configuration. Furthermore, for this configuration a wide data variance between the different measurements is observed, this means that the reaction yield was not stable over time with particles being periodically pushed out of the reactor, indicating particle agglomeration and onset of channel clogging (see Table 2). Despite the concentrated acoustic pressure distribution at the box surface (Figure 8b), operating the six transducers at 80kHz might

not deliver enough cavitation energy to break up particle agglomerates. This could be as smaller cavitation bubbles at higher frequencies have a weaker mechanical effect and do not initiate micro-turbulence as violently as larger cavitating bubbles nucleated at lower frequencies. The particle size distribution of the 6tr-40 and 6tr-40/80 configurations is relatively similar, with the smallest mean size and span observed in the 6tr-40 configuration. This similarity between these two configurations could be explained by the presence of a transducer operated at 40kHz at the reactor outlet in the 6tr-40/80 configuration. Due to the enhanced cavitation activity provided by 40kHz transducers the formed particle agglomerates are broken up by this last transducer in the reactor assembly. A similar effect was observed by Delacour *et al.*¹ when applying pulsed ultrasound to the barium sulfate precipitation in a microreactor, where it was found that particles experiencing two pulses of 5s of ultrasound were smaller compared to particles only experiencing a single pulse of 10s. However, only the 6tr-40 configuration resulted in a high yield with narrow variance between measurements (see Table 2) meaning that particles were constantly leaving the reactor over time. Therefore, the actuation frequency of 40kHz was used to study the effect of transducer configuration.



Configuration	Dv(10)(μm)	Dv(50)(μm)	Dv(90)(μm)	Dv(90-10)(μm)
Silent	2.76 \pm 0.06	7.42 \pm 0.88	23.5 \pm 3.39	20.7 \pm 0.34
6tr-40	1.67 \pm 0.07	3.47 \pm 0.16	6.53 \pm 0.46	4.87 \pm 0.41
6tr-80	2.21 \pm 0.39	4.99 \pm 0.75	11.7 \pm 0.86	9.49 \pm 0.66
6tr-40/80	1.88 \pm 0.20	4.01 \pm 0.39	8.22 \pm 0.98	6.35 \pm 1.36

Figure 9. Effect of frequency configuration on the particle size distribution (Dv(X)) of barium sulfate. Results obtained at a flow rate of 2mL/min, a concentration of 0.5M and a load power per transducer of 20W.

Table 2. Effect of the frequency configuration on the average yield of the barium sulfate precipitation reaction. The results are obtained at a flow rate of 2mL/min, a concentration of 0.5M and a load power per transducer of 20W.

Configuration	6tr-40	6tr-80	6tr-40/80
Yield (%)	71.0±9.0	72.0±14.4	67.7±18.2

3.3. Effect of the transducer configuration on the barium sulfate precipitation reaction

To investigate the effect of the transducer configuration on the acoustic pressure field distribution and on the barium sulfate precipitation reaction, experiments were conducted at a frequency of 40kHz and 20W load power per transducer for the 6tr-40, 2tr-IO, 2tr-M and 4tr configurations (see Figure 4).

Figure 10 depicts the acoustic pressure distribution in the reactor cavity obtained by COMSOL simulations. It can be noticed that a higher pressure is obtained near the wall for the 6tr-40 configuration compared to the other three cases. In addition, the acoustic pressure distribution is quite uniform over the entire length of the reactor for the 2tr-IO and 4tr cases. For the 2tr-M configuration a low acoustic pressure is observed at the inlet and outlet of the reactor, which could lead to a lower cavitation activity in that reactor volume.

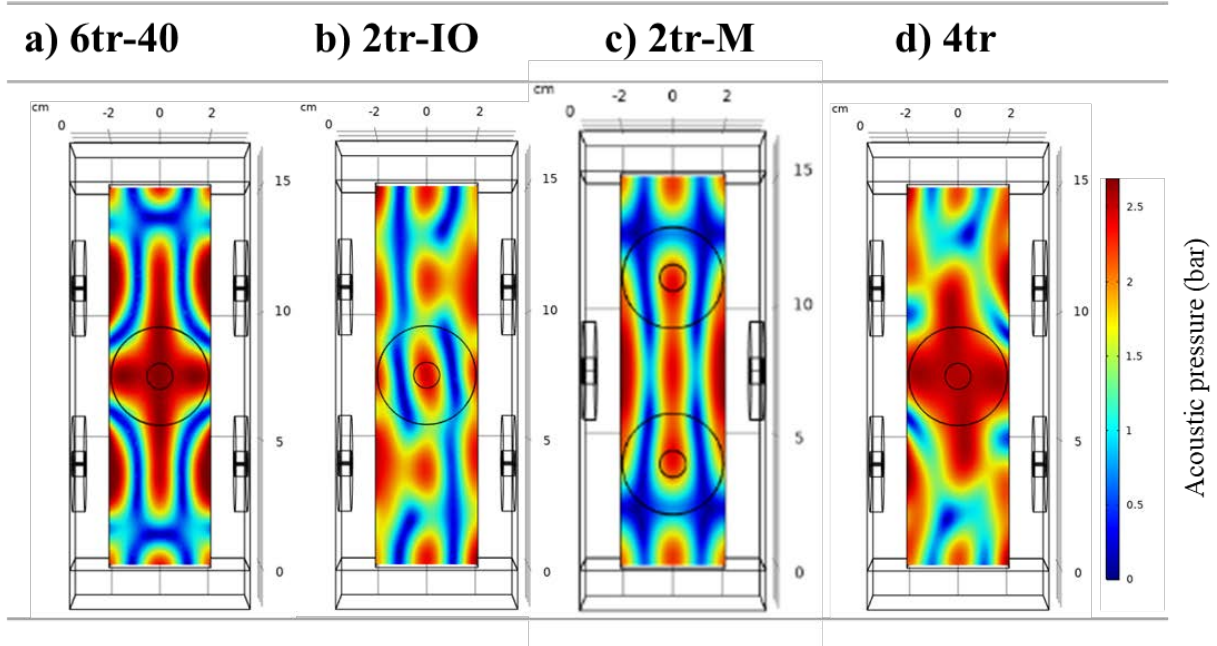
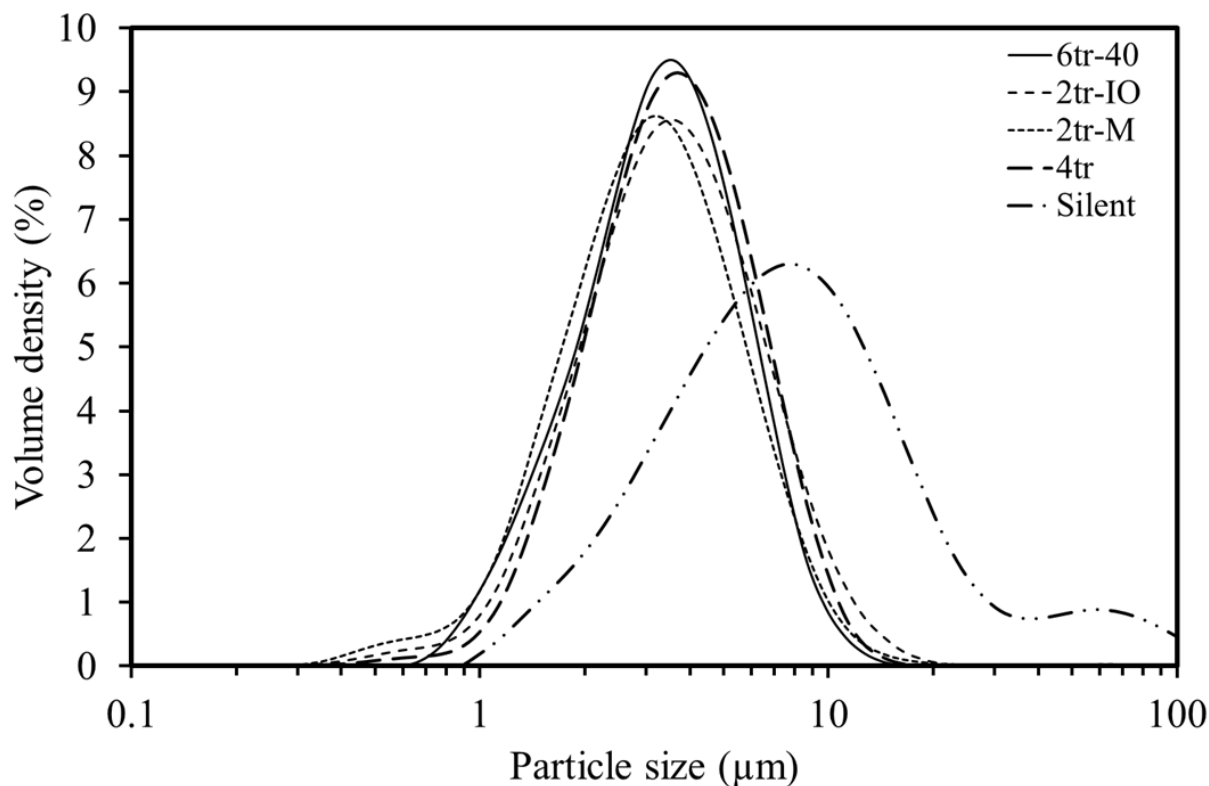


Figure 10. Contours of the acoustic pressure field based on COMSOL simulations for a power of 20W per transducer obtained using $\beta = 4 \cdot 10^{-7}$ as void fraction. (a) 2TR plane for 6tr-40, (b) 2TR plane for 2tr-IO, (c) 1TR plane for 2tr-M (d) 2TR plane for 4tr.

The experimentally obtained particle size distributions for the four different transducer configurations and the silent condition are shown in Figure 11. As observed previously, upon ultrasound irradiation smaller mean particle sizes and narrower particle size distributions are obtained. It can be seen from the data in Figure 11 that the particle size distributions are quite similar for each transducer configuration.



Configuration	Dv(10) (μm)	Dv(50) (μm)	Dv(90) (μm)	Dv(90-10) (μm)
Silent	2.76±0.06	7.42±0.88	23.5±3.39	20.7±0.34
6tr-40	1.67±0.07	3.47±0.16	6.53±0.46	4.87±0.41
2tr-IO	1.77±0.12	3.83±0.18	7.90±0.41	6.13±0.41
2tr-M	1.59±0.12	3.43±0.31	7.04±0.71	5.45±0.61
4tr	1.90±0.21	3.87±0.44	7.95±1.48	6.05±1.36

Figure 11. Effect of the transducer configuration on the particle size distribution (Dv(X)) of the barium sulfate precipitation reaction. Results obtained at a flow rate of 2mL/min, a concentration of 0.5M, a frequency of 40kHz and a load power per transducer of 20W.

The main difference between the configurations is found when characterizing the reaction yield (see Table 3). The two configurations resulting in high yields and low deviation are the 6tr-40 and the 4tr configurations. For the 2tr-IO configuration, a high deviation between yield values is

obtained which means that the yield was fluctuating. Moreover, it was observed that particles were frequently pushed out of the reactor. This unstable yield and reactor behavior might be due to the lower acoustic pressure in the reactor cavity resulting in a lower cavitation activity (Figure 10b). The lowest yield value is obtained for the 2tr-M configuration. This might be due to the low cavitation activity at the inlet and outlet resulting in a particle accumulation (Figure 10c). Consequently, the 2tr-IO and 2tr-M configurations might lead to channel clogging, and thus only the 6tr-40 and 4tr configurations result in a stable process. The difference between the latter two configurations is the narrower particle size distribution obtained for 6tr-40. The clogging prevention potential of the 6tr-40 configuration was investigated by performing a longer experiment with an operation time of 114min (equivalent to 18 reactor volume). A stable yield over time was observed, highlighting that no clogging occurred in this longer experiment. In conclusion, this parameter study showed the versatility of the reactor to produce small sized particles in a continuous flow reactor, without channel clogging.

Table 3. Effect of the transducer configuration on the average yield of the barium sulfate precipitation reaction. The results are obtained at a flow rate of 2mL/min, a concentration of 0.5M a frequency of 40kHz and a load power per transducer of 20W.

Configuration	6tr-40	2tr-IO	2tr-M	4tr
Yield (%)	71.0±9.0	81.2±24.8	67.9±7.2	72.1±3.6

3.4. Quantification of the scale-up from a ultrasonic microreactor

The designed scaled-up ultrasonic millireactor (USMR) in the 6tr-40 configuration is compared to a previously studied ultrasonic microreactor (US μ R)¹. The US μ R consists of a silicon-based microfluidic chip directly attached to a Langevin's type transducer, and Table 4 compares the

different reactor characteristics. Table 5 lists the characteristic dimensions of the experimentally obtained particle size distributions.

Table 4. Characteristics of the ultrasonic microreactor (US μ R) and the scaled-up ultrasonic millireactor (USMR) applied to the barium sulfate precipitation reaction.

Parameter	Ultrasonic (USμR)	micro-reactor	Ultrasonic (USMR)	milli-reactor
Volume (mL)	0.513		12	
Residence time (min)	1.33		6	
Flow rate (mL/min)	0.2		2	
Concentration (M)	0.043		0.5	
Productivity (g/h)	0.12		14	
Load power per volume (W/mL)	38		0.48	
Frequency (kHz)	21		40	
Channel characteristics	Square channel: 0.6mm ²		2mm inner diameter tubing	

Table 5. Comparison of the characteristic dimensions $D_v(X)$ of the volume-based particle size distribution obtained in the US μ R at a flow rate of 0.2mL/min, a concentration of 0.043M, a load power of 38W/mL, and a frequency of 21kHz and in the USMR at a flow rate of 2mL/min, a concentration of 0.5M, a load power of 0.48W/mL and a frequency of 40kHz.

Reactor	$D_v(10)(\mu\text{m})$	$D_v(50)(\mu\text{m})$	$D_v(90)(\mu\text{m})$	$D_v(90-10)(\mu\text{m})$
USμR	2.6 \pm 0.64	6.1 \pm 1.39	18.4 \pm 2.12	15.8 \pm 1.48
USMR	1.67 \pm 0.07	3.47 \pm 0.16	6.53 \pm 0.46	4.87 \pm 0.41

Compared to the US μ R, the scale-out approach used in this study allowed to increase the volume from 0.513 to 12mL, also allowing an increase by an order of magnitude in the flow rate and the concentration to 2mL/min and 0.5M respectively. Hence, the scaled-up reactor results in a two order of magnitude increased productivity, from 0.12 to 14g/h. In addition to this large increase in productivity, no clogging was observed which further proves the feasibility of the scaled-up reactor for handling solid particles. These results are obtained at a load power per volume of 0.48W/mL in the USMR, significantly lower compared to the US μ R with a load power per volume of 38W/mL. Thus, the scaled-up reactor is operated in an energy efficient manner, which also limits the temperature increase of the reaction mixture due to ultrasound irradiation. Furthermore, the scaled-up reactor results in smaller mean particles and narrower particle size distributions. While the reaction is performed at different frequencies, 21kHz for the US μ R and 40kHz for the USMR, earlier studies showed that particles sizes are not majorly affected by frequency^{1,40,41}. Secondly, to understand the different size distribution between the US μ R and the USMR, two parameters have to be considered: the flow rate and the residence time. Increasing the flow rate from 0.2mL/min in the US μ R to 2mL/min in the USMR results in a better mixing efficiency⁴². Then, the decrease in particle sizes can be explained by the increase in residence time from 80s in the US μ R to 6min in the USMR. An increase in residence time means an increase in the contact time between particles and the acoustic effects such as sonofragmentation. Nevertheless, the results obtained in the designed scaled-up reactor highlight that particle synthesis without clogging is performed at increased productivity and at lower load power per volume, further validating the scale-out approach.

4. Conclusions

A novel scaled-up ultrasonic millireactor was developed in this work. Its application to the synthesis of barium sulfate revealed that a low load power per volume of 0.48W/mL was required to prevent channel clogging and to increase the productivity by two orders of magnitude compared to a microreactor. The designed reactor is flexible in actuation frequency and transducer configuration, and the combined numerical and experimental characterization revealed that operating at 40kHz and with all transducers active resulted in an acoustic wave distribution with maximum acoustic pressures in the vicinity of the tubular reactor, thus leading to a narrow particle size distribution and clogging prevention for the studied model reaction. Moreover, the investigation of the different frequency configurations reveals the necessity to use a transducer operating at 40kHz close to the outlet of the reactor, due to a weaker cavitation activity obtained at 80kHz. Experiments on the impact of the transducer configurations showed that the acoustic pressure mapping was closely related to the yield stability over time. The present study highlights the importance of developing experimental and numerical characterization methods of the ultrasound and cavitation effect for the design of scaled-up ultrasonic millireactors.

References

- (1) Delacour, C.; Lutz, C.; Kuhn, S. Pulsed Ultrasound for Temperature Control and Clogging Prevention in Micro-Reactors. *Ultrason. Sonochem.* **2019**, *55*, 67–74.
<https://doi.org/10.1016/j.ultsonch.2019.03.012>.
- (2) Dong, Z.; Fernandez Rivas, D.; Kuhn, S. Acoustophoretic Focusing Effects on Particle Synthesis and Clogging in Microreactors. *Lab Chip* **2019**, *19*, 316–327.
<https://doi.org/10.1039/c8lc00675j>.
- (3) Pohl, B.; Jamshidi, R.; Brenner, G.; Peuker, U. A. Experimental Study of Continuous Ultrasonic Reactors for Mixing and Precipitation of Nanoparticles. *Chem. Eng. Sci.* **2012**, *69*, 365–372. <https://doi.org/10.1016/j.ces.2011.10.058>.
- (4) Dodds, J. A.; Espitalier, F.; Louisnard, O.; Grossier, R.; David, R.; Hassoun, M.; Baillon, F.; Gatumel, C.; Lyczko, N. The Effect of Ultrasound on Crystallisation-Precipitation Processes : Some Examples and a New Segregation Model. *Part. Part. Syst. Charact.* **2007**, *24*, 18–28. <https://doi.org/10.1002/ppsc.200601046>.
- (5) Gielen, B.; Thimmesch, Y.; Jordens, J.; Janssen, G.; Thomassen, L. C. J.; Van Gerven, T.; Braeken, L. Ultrasonic Precipitation of Manganese Carbonate: Reactor Design and Scale-Up. *Chem. Eng. Res. Des.* **2016**, *115*, 131–144.
<https://doi.org/10.1016/j.cherd.2016.09.012>.
- (6) Castro, F.; Kuhn, S.; Jensen, K.; Ferreira, A.; Rocha, F.; Vicente, A.; Teixeira, J. A. Continuous-Flow Precipitation of Hydroxyapatite in Ultrasonic Microsystems. *Chem. Eng. J.* **2013**, *215–216*, 979–987. <https://doi.org/10.1016/j.cej.2012.11.014>.
- (7) Dong, Z.; Udepurkar, A. P.; Kuhn, S. Synergistic Effects of the Alternating Application of Low and High Frequency Ultrasound for Particle Synthesis in Microreactors. *Ultrason.*

- Sonochem.* **2020**, *60*, 104800. <https://doi.org/10.1016/j.ultsonch.2019.104800>.
- (8) Hussain, M. N.; Jordens, J.; John, J. J.; Braeken, L.; Van Gerven, T. Enhancing Pharmaceutical Crystallization in a Flow Crystallizer With Ultrasound: Anti-Solvent Crystallization. *Ultrason. Sonochem.* **2019**, *59*, 104743. <https://doi.org/10.1016/j.ultsonch.2019.104743>.
- (9) Kuhn, S.; Noël, T.; Gu, L.; Heider, P. L.; Jensen, K. F. A Teflon Microreactor with Integrated Piezoelectric Actuator to Handle Solid Forming Reactions. *Lab Chip* **2011**, *11* (15), 2488–2492. <https://doi.org/10.1039/c1lc20337a>.
- (10) Noël, T.; Naber, J. R.; Hartman, R. L.; McMullen, J. P.; Jensen, K. F.; Buchwald, S. L. Palladium-Catalyzed Amination Reactions in Flow: Overcoming the Challenges of Clogging via Acoustic Irradiation. *Chem. Sci.* **2011**, *2*, 287–290. <https://doi.org/10.1039/C0SC00524J>.
- (11) Hartman, R. L.; Naber, J. R.; Zaborenko, N.; Buchwald, S. L.; Jensen, K. F. Overcoming the Challenges of Solid Bridging and Constriction during Pd-Catalyzed C-N Bond Formation in Microreactors. *Org. Process Res. Dev.* **2010**, *14*, 1347–1357. <https://doi.org/10.1021/op100154d>.
- (12) Yaseneva, P.; Hodgson, P.; Zakrzewski, J.; Falß, S.; Meadows, R. E.; Lapkin, A. A. Continuous Flow Buchwald–Hartwig Amination of a Pharmaceutical Intermediate. *React. Chem. Eng.* **2016**, *1*, 229–238. <https://doi.org/10.1039/C5RE00048C>.
- (13) Shu, W.; Pellegatti, L.; Oberli, M. A.; Buchwald, S. L. Continuous-Flow Synthesis of Biaryls Enabled by Multistep Solid-Handling in a Lithiation/Borylation/Suzuki-Miyaura Cross-Coupling Sequence. *Angew. Chemie - Int. Ed.* **2011**, *50*, 10665–10669. <https://doi.org/10.1002/anie.201105223>.

- (14) Sedelmeier, J.; Ley, S. V.; Baxendale, I. R.; Baumann, M. KMnO(4)-Mediated Oxidation as a Continuous Flow Process. *Org. Lett.* **2010**, *12* (16), 3618–3621.
<https://doi.org/10.1021/ol101345z>.
- (15) Dong, Z.; Delacour, C.; Mc Carogher, K.; Udepurkar, A. P.; Kuhn, S. Continuous Ultrasonic Reactors: Design, Mechanism and Application. *Materials (Basel)*. **2020**, *13*, 344. <https://doi.org/10.3390/ma13020344>.
- (16) John, J. J.; Kuhn, S.; Braeken, L.; Van Gerven, T. Temperature Controlled Interval Contact Design for Ultrasound Assisted Liquid–Liquid Extraction. *Chem. Eng. Res. Des.* **2017**, *125*, 146–155. <https://doi.org/10.1016/j.cherd.2017.06.025>.
- (17) Kuijpers, K. P. L.; Van Dijk, M. A. H.; Rumeur, Q. G.; Hessel, V.; Su, Y.; Noël, T. A Sensitivity Analysis of a Numbered-up Photomicroreactor System. *React. Chem. Eng.* **2017**, *2*, 109–115. <https://doi.org/10.1039/c7re00024c>.
- (18) Qiu, M.; Zha, L.; Song, Y.; Xiang, L.; Su, Y. Numbering-up of Capillary Microreactors for Homogeneous Processes and Its Application in Free Radical Polymerization. *React. Chem. Eng.* **2019**, *4* (2), 351–361. <https://doi.org/10.1039/c8re00224j>.
- (19) van Zwieten, R.; Verhaagen, B.; Schroën, K.; Fernández Rivas, D. Emulsification in Novel Ultrasonic Cavitation Intensifying Bag Reactors. *Ultrason. Sonochem.* **2017**, *36*, 446–453. <https://doi.org/10.1016/j.ultsonch.2016.12.004>.
- (20) Verhaagen, B.; Liu, Y.; Pérez, A. G.; Castro-Hernandez, E.; Fernandez Rivas, D. Scaled-up Sonochemical Microreactor with Increased Efficiency and Reproducibility. *ChemistrySelect* **2016**, *2*, 136–139. <https://doi.org/10.1002/slct.201600023>.
- (21) Rivas, D. F.; Verhaagen, B.; Perez, A. G.; Castro-Hernandez, E.; Van Zwieten, R.; Schroen, K. A Novel Ultrasonic Cavitation Enhancer. *J. Phys. Conf. Ser.* **2015**, *656*

- (012112). <https://doi.org/10.1088/1742-6596/656/1/012112>.
- (22) Ezeanowi, N.; Pajari, H.; Laitinen, A.; Koiranen, T. Monitoring the Dynamics of a Continuous Sonicated Tubular Cooling Crystallizer. *Cryst. Growth Des.* **2020**, *20* (3), 1458–1466. <https://doi.org/10.1021/acs.cgd.9b01103>.
- (23) Ezeanowi, N.; Koiranen, T. Effect of Process Parameters on a Novel Modular Continuous Crystallizer. In *International Process Intensification Conference 2019*; 2019.
- (24) Karvonen, V.; Häkkinen, A.; Louhi-Kultanen, M.; Koiranen, T. Method and Apparatus for Continuous Crystallization and Use Thereof. WO 2016/107968 AI, 2016.
- (25) Gogate, P. R.; Pandit, A. B. Sonochemical Reactors: Scale up Aspects. *Ultrason. Sonochem.* **2004**, *11*, 105–117. <https://doi.org/10.1016/j.ultsonch.2004.01.005>.
- (26) Navarro-Brull, F. J.; Poveda, P.; Ruiz-Femenia, R.; Bonete, P.; Ramis, J.; Gómez, R. Guidelines for the Design of Efficient Sono-Microreactors. *Green Process. Synth.* **2014**, *3*, 311–320. <https://doi.org/10.1515/gps-2014-0052>.
- (27) Gogate, P. R.; Sutkar, V. S.; Pandit, A. B. Sonochemical Reactors: Important Design and Scale up Considerations with a Special Emphasis on Heterogeneous Systems. *Chem. Eng. J.* **2011**, *166*, 1066–1082. <https://doi.org/10.1016/j.cej.2010.11.069>.
- (28) Sutkar, V. S.; Gogate, P. R. Design Aspects of Sonochemical Reactors: Techniques for Understanding Cavitation Activity Distribution and Effect of Operating Parameters. *Chem. Eng. J.* **2009**, *155*, 26–36. <https://doi.org/10.1016/j.cej.2009.07.021>.
- (29) Jordens, J.; Honings, A.; Degève, J.; Braeken, L.; Van Gerven, T. Investigation of Design Parameters in Ultrasound Reactors with Confined Channels. *Ultrason. Sonochem.* **2013**, *20*, 1345–1352. <https://doi.org/10.1016/j.ultsonch.2013.03.012>.
- (30) Jamshidi, R.; Rossi, D.; Saffari, N.; Gavriilidis, A.; Mazzei, L. Investigation of the Effect

- of Ultrasound Parameters on Continuous Sonocrystallization in a Millifluidic Device. *Cryst. Growth Des.* **2016**, *16*, 4607–4619. <https://doi.org/10.1021/acs.cgd.6b00696>.
- (31) Sarac, B. E.; Stephens, D. S.; Eisener, J.; Rosseló, J. M.; Mettin, R. Cavitation Bubble Dynamics and Sonochemiluminescence Activity inside Sonicated Submerged Flow Tubes. *Chem. Engineering Process. Intensification* **2019**, 100632. <https://doi.org/10.1016/j.cep.2020.107872>.
- (32) Tandiono; Ohl, S.-W.; Ow, D. S. W.; Klaseboer, E.; Wong, V. V.; Dumke, R.; Ohl, C.-D. Sonochemistry and Sonoluminescence in Microfluidics. *PNAS* **2011**, *108* (15), 5996–5998. <https://doi.org/10.1073/pnas.1019623108>.
- (33) Rossi, D.; Jamshidi, R.; Saffari, N.; Kuhn, S.; Gavriilidis, A.; Mazzei, L. Continuous-Flow Sonocrystallization in Droplet-Based Microfluidics. *Cryst. Growth Des.* **2015**, *15*, 5519–5529. <https://doi.org/10.1021/acs.cgd.5b01153>.
- (34) Louisnard, O. A Simple Model of Ultrasound Propagation in a Cavitating Liquid. Part I: Theory, Nonlinear Attenuation and Traveling Wave Generation. *Ultrason. Sonochem.* **2012**, *19* (1), 66–76. <https://doi.org/10.1016/j.ultsonch.2011.06.008>.
- (35) Louisnard, O. A Simple Model of Ultrasound Propagation in a Cavitating Liquid. Part II: Primary Bjerknes Force and Bubble Structures. *Ultrason. Sonochem.* **2012**, *19* (1), 56–65. <https://doi.org/10.1016/j.ultsonch.2011.06.007>.
- (36) Jamshidi, R.; Pohl, B.; Peuker, U. A.; Brenner, G. Numerical Investigation of Sonochemical Reactors Considering the Effect of Inhomogeneous Bubble Clouds on Ultrasonic Wave Propagation. *Chem. Eng. J.* **2012**, *189–190*, 364–375. <https://doi.org/10.1016/j.cej.2012.02.029>.
- (37) Hussain, M. N.; Janajreh, I. Numerical Simulation and Experimental Testing of Novel

- Sonochemical Reactor for Transesterification. *Waste and Biomass Valorization* **2017**, *8* (5), 1733–1747. <https://doi.org/10.1007/s12649-017-9960-7>.
- (38) van Iersel, M. M.; Benes, N. E.; Keurentjes, J. T. F. Importance of Acoustic Shielding in Sonochemistry. *Ultrason. Sonochem.* **2008**, *15*, 294–300. <https://doi.org/10.1016/j.ultsonch.2007.09.015>.
- (39) Fernandez Rivas, D.; Kuhn, S. Synergy of Microfluidics and Ultrasound: Process Intensification Challenges and Opportunities. *Top. Curr. Chem.* **2016**, *374* (70). <https://doi.org/10.1007/s41061-016-0070-y>.
- (40) Lee, J.; Ashokkumar, M.; Kentish, S. E. Influence of Mixing and Ultrasound Frequency on Antisolvent Crystallisation of Sodium Chloride. *Ultrason. - Sonochemistry* **2014**, *21*, 60–68. <https://doi.org/10.1016/j.ultsonch.2013.07.005>.
- (41) Jordens, J.; De Coker, N.; Gielen, B.; Van Gerven, T.; Braeken, L. Ultrasound Precipitation of Manganese Carbonate: The Effect of Power and Frequency on Particle Properties. *Ultrason. Sonochem.* **2015**, *26*, 64–72. <https://doi.org/10.1016/j.ultsonch.2015.01.017>.
- (42) Gobert, S. R. L.; Kuhn, S.; Braeken, L.; Thomassen, L. C. J. Characterization of Milli- and Microflow Reactors: Mixing Efficiency and Residence Time Distribution. *Org. Process Res. Dev.* **2017**, *21* (4), 531–542. <https://doi.org/10.1021/acs.oprd.6b00359>.